Single-walled Carbon Nanotube Membranes Accelerate Active Osteogenesis in Bone Defects: Potential of Guided Bone Regeneration Membranes

Yikun Xu,[†] Eri Hirata,[†] Yoko Iizumi,[§] Natsumi Ushijima,[†] Keisuke Kubota,[†] Sadahito Kimura,[†]*

Yukari Maeda,[†] Toshiya Okazaki,[§] and Atsuro Yokoyama[†]

[†] Graduate School of Dental Medicine, Hokkaido University, Sapporo 060-8586, Japan

[§] Nanomaterials Research Institute (NMRI), National Institute of Advanced Industrial Science and Technology (AIST), Tsukuba Central, Tsukuba 305-8565, Japan

Corresponding author. Tel: +81-11-706-4270 Fax: +81-11-706-4903

E-mail address: erieri@den.hokudai.ac.jp *(E. Hirata)

ORCID iD : 0000-0001-6718-1465

Abstract

Carbon nanotubes (CNTs) are potentially important biomaterials because of their chemical, physical, and biological properties. Our research indicates CNTs exhibit high compatibility with bone tissue. The guided bone regeneration (GBR) technique is commonly applied to reconstruct alveolar bone and treat peri-implant bone defects. In GBR, bone defects are covered with a barrier membrane to prevent entry of non-osteogenic cells such as epithelial cells and fibroblasts. The barrier membrane also maintains a space for new bone formation. However, the mechanical and biological properties of materials previously used in clinical practice sometimes delayed bone regeneration. In this study, we developed a CNT-based membrane for GBR exhibiting high strength to provide a space for bone formation and provide cellular shielding to induce osteogenesis. The CNT membrane was made via dispersion of single-walled CNTs (SWCNTs) in hyaluronic acid solution followed by filtration. The CNT membrane assumed a nanostructure surface due to the bundled SWCNTs and exhibited high strength and hydrophilicity after oxidation. In addition, the membrane promoted the proliferation of osteoblasts but not non-osteogenic cells. CNT membranes were used to cover experimental bone defects made in rat calvaria. At 8 weeks after surgery, more extensive bone formation was observed in membrane-covered defects compared with bone defects not covered with membrane. Almost no diffusion of CNTs was observed around the membrane. These results indicate that the CNT membrane has adequate strength, stability, and surface characteristics for osteoblasts, and its shielding properties promote bone formation. Demonstration of the safety and osteogenic potential of the CNT membranes through further animal studies should facilitate their clinical application in GBR.

Keywords

Single-walled carbon nanotube, Guided bone regeneration (GBR), Osteoblast, Bone formation

Introduction

Carbon nanotubes (CNTs) are sp^2 carbon bonded tubular materials first reported by Iijima et al.[1,2]. There are two main types of CNTs, single-walled carbon nanotubes (SWCNTs) and multi-walled carbon nanotube (MWCNTs). CNTs have been extensively studied in biomedicine because of their physical and chemical properties, unique structure, biocompatibility, and low toxicity[3–7]. Usui et al.[8] reported that MWCNTs accelerate bone formation and are highly compatible with bone tissue. Barrientos-Durán et al.[9] found that culturing human preosteoblasts and murine embryonic stem cells on SWCNTs accelerated their osteogenic differentiation. We previously reported that MWCNT-coated substrates provide enhanced osteoblast adhesion and differentiation and have a favorable bone compatibility profile[10–12]. MWCNT-coated collagen sponges loaded with growth factors provide controlled release and promote bone regeneration[13].

Guided bone regeneration (GBR) is one of the most common treatment approaches for reconstructing alveolar bone and treating peri-implant bone defects. In GBR, a barrier membrane is applied to cover the bone defects and prevent the entry of non-osteogenic cells such as epithelial cells and fibroblasts[14–16]. The membrane also maintains a space for new bone formation. Murray et al.[17] reported that shielding the bone defect from the surrounding tissue accelerates bone healing. The GBR technique is widely used for treating defects in the maxillofacial area, and the membrane materials used for GBR have been extensively researched. To be effective, GBR membranes should exhibit biocompatibility, high mechanical strength, and surgical maneuverability[14]. Numerous materials have been studied as potential GBR membranes, including natural polymers such as collagen, chitosan, and silk

fibroin; metal alloys of titanium, magnesium, and zinc; and synthetic polymers such as polytetrafluoroethylene (PTFE). However, because PTFE is a non-resorbable material, it does not have sufficient strength and hydrophilicity to be treated with proteins such as growth factors. Although collagen and chitosan are resorbable materials, they also have insufficient strength and can cause inflammation upon resorption. Therefore, the inadequate mechanical and biological properties of these materials can result in delayed bone regeneration in clinical practice[17,18].

To develop more-effective GBR membranes, we previously prepared carbon nanohorns (CNHs), a type of carbon nanomaterial, and adhered them to PTFE membranes. We found that membranes with CNHs promoted bone regeneration[19] and that CNHs accelerated osteoblast differentiation via macrophage activation[20]. However, the strength of the CNH membranes was weak due to their adherence to PTFE, and some of the CNHs detached from the membrane surface. We hypothesized that these problems could be overcome by exploiting the characteristic nanostructure surface, high mechanical strength, and large surface area of SWCNTs (0.5-2.0 nm in diameter and >100 nm to several centimeters in length)[21,22] and using them as independent membranes without a PTFE lining. In the present study, SWCNTs were dispersed in hyaluronic acid (HA) to prepare HACNT membranes. The morphological structure and mechanical properties of the HACNT membranes were investigated, as well as their potential to inhibit the proliferation of non-osteogenic cells and promote that of osteoblasts, which are essential factors for successful GBR treatment. The tissue response and bone regeneration ability were also evaluated, and the dispersion of CNTs in surrounding tissues was surveyed using Raman spectroscopy.

The results of the present study demonstrate that HACNT membranes exhibit high strength and hydrophilicity and inhibit the proliferation of non-osteogenic cells but promote osteoblast proliferation. Furthermore, extensive osteogenesis in experimental bone defects in rat calvaria was observed, with almost no diffusion of CNTs into the tissue around the membrane.

Results and Discussion

Figure 1a-e shows the results of characterization of the HACNT membrane. The HACNT formed a black film as shown in Figure 1a. The nanostructured surface with a characteristic bundled structure of SWCNTs was observed by scanning electron microscopy (SEM), as shown in Figure 1b. Figure 1c shows a photograph of measurement of the water contact angle (CA) of the HACNT membrane, which was 10°–16°. The characteristics of the HACNT membrane were compared to those of PTFE membranes, which are already in clinical use. Zhang et al. reported that the CA of PTFE is approximately 118° [23]. Even before oxidation, the CA of the HACNT film was 25° and decreased further after oxidation by treatment with a UV ozone cleaner. In addition, the tensile strength and Young's modulus of the PTFE membrane was 32 N/mm^2 and 203 N/mm^2 (Figure 1d), whereas that of the HACNT membrane was 202 N/mm^2 and 7330 N/mm^2 (Figure 1e). These results demonstrate that the hydrophilicity and strength of CNT membranes are much higher than those of PTFE membranes.

The GBR membrane covering a bone defect acts to prevent invasion of the defect by non-osteogenic cells such as epithelial cells and fibroblasts while promoting the proliferation of the osteoblastic cells that form new bone in the space under the membrene[14,15]. In this study, the proliferation of three types of cells was examined. Figure 2Aa-c and Ba-c shows the proliferation of a mouse calvaria osteoblastic cell line (MC3T3-E1), mouse embryonic fibroblast cell line (NIH/3T3), and human gingival carcinoma epithelial-like cell line (Ca9-22). SEM observations showed that the pseudopodia of MC3TC-E1 cells were more extended and entangled with the CNT membrane than the other types of cells (Figure 2Aa-c). Remarkably, on the HACNT membrane, the number of osteoblasts

increased significantly, as indicated by an increase in DNA content from day 3 to day 7 (Figure 2Ba). In contrast, no increase in the number of fibroblasts (Figure 2Bb) or epithelial cells (Figure 2Bc) was observed. Moreover, the pseudopodia of MC3T3-E1 were entangled in CNTs after 4 hours, but the pseudopodia of Ca9-22 and NIH3T3 were not entangled in CNTs (Figure S4A). 24 hours later, all cells proliferated compared to 4 hours later. In particular, MC3T3-E1 cells were tightly spread across the HACNT membrane, and there were few gaps between the cells and the membrane as seen in Ca9-22 and NIH3T3 (Figure S4B). These initial cell adhesion state differences may affect cell proliferation, causing osteoblasts to proliferate while epithelial cells and fibroblasts are less likely to proliferate.

The surface properties of the membrane material, including its hydrophilicity and roughness, have a significant impact on cell proliferation and attachment[24]. The HACNT membrane consisted of SWCNTs with a diameter of 1.5 nm, and the CA was 10°–16°, indicating the membrane has a specific nanostructure and high hydrophilicity. Several studies have shown that hydrophilic surfaces can promote the growth, adhesion, and proliferation of osteoblasts[24,25], fibroblasts[26], and epithelial cells[27]. High hydrophilicity and a high degree of roughness of the material surface promote the selective adsorption of fibrinogen and fibronectin, two critical regulators of osteoblast adhesion and proliferation[25,28]. However, in the present study, the number of fibroblasts and epithelial cells on HACNT membranes did not increase to the same degree as cells plated in cell culture dishes. The difference in proliferation of these cells on the HACNT membrane could be due to the surface roughness. Several studies have shown that a nanotopographic surface structure promotes the osteogenic

differentiation of dental pulp stem cells[29] and that osteoblasts proliferate well on rough surfaces[24], whereas fibroblasts and epithelial cells proliferate better on smooth surfaces. Kunzler et al. reported a significant increase in the proliferation rate of osteoblasts with increasing surface roughness, whereas fibroblasts exhibited the opposite proliferative behavior, with the proliferation rate decreasing with increasing roughness[30]. Baharloo et al. demonstrated a decrease in epithelial cell proliferation when cells were seeded on a rough surface compared to a smooth surface[31]. Therefore, the hydrophilicity and specific nanostructure of HACNT membranes could promote cell adhesion and osteoblast proliferation, although the nanoscale surface structure could inhibit fibroblast and epithelial cell proliferation.

This study used HA to disperse and bind SWCNTs to generate the finished membrane configuration. HA is a natural component of the human body utilized in drugs and biomaterials such as viscosupplementation agents and bioscaffolds[32–34]. The safety of HA for these applications has been demonstrated. The calculated HA content in the HACNT membrane was 7.7wt% (Figure S1). Figure S2 shows the DNA content and alkaline phosphatase (ALP) activity of mouse bone marrow stromal cells cultured for 7 days in the presence of various concentrations of HA. Neither the DNA content nor ALP activity changed, even when the concentration of hyaluronan was increased to 0.5 mg/mL. These results suggest that elution of HA from the HACNT membrane does not adversely affect cell proliferation or differentiation.

Figure 3 shows the results of micro–computed tomography (μ-CT) analyses of bone regeneration in calvarial bone defects after 8 weeks in rats with/without HACNT membrane covering. As shown in Figure 3A,

more-extensive and thicker radiopaque images were observed in the HACNT membrane group (Figure 3Ab, d, and f) compared with the control group lacking membrane covering of the defect (Figure 3Aa, c, and e). Figure 3B shows a schematic illustration of the method for measuring new bone production in the defect area. The volume of new bone in the HACNT membrane group was significantly higher than that in the control group, as determined by μ-CT analyses (Figure 3C).

Figure 4 shows the results of histologic analyses of the two groups. At 8 weeks, new bone (black asterisks) was formed from the edge of the existing calvarial bone (EB). Some of the new bone was seen apart from the existing bone (Figure 4Aa). The newly formed bone had lamellar structures (black arrow) (Figure 4Ab), and fibrous connective tissue, including fibroblasts, was observed around the newly formed bone. These results indicate that the process of bone regeneration in the control group had finished. In contrast, more-extensive bone formation was observed under the HACNT membrane (yellow arrowhead) (Figure 4Ba) compared with the control group (Figure 4Aa). A portion of the HACNT membrane (pink arrowhead) was folded on the newly formed bone (Figure 4Ba). The new bone formed continuously along the edge of the calvaria. Many osteoblasts with large nucleus and rectangle large cell body (white arrowheads) were lined on the surface of the upper part of the newly formed bone, and cells with large and slightly bright cytoplasm like mesenchymal cells (black arrowheads), and capillaries (white arrows) indicative of active osteogenesis were observed around new bone tissue (Figure 4Bb). Simultaneously, lamellar structures (black arrows) were seen only in the lower part of the newly formed bone along with the dura (Figure 4Ba). A lamellar structure indicative of stable bone remodeling

was seen in the control group. However, a variety of cells, such as mesenchymal cells with (black arrowheads), fibroblasts, macrophages, and capillaries (white arrows), were identified under the HACNT membrane (Figure 4Bc), indicating that the HACNT membrane induces high regenerative activity even in the late stages of tissue repair.

Significantly, many large cells, such as mesenchymal cells (black arrowheads), were observed close to the membrane, confirming that the specific surface nanostructure of the SWCNTs in the membrane promotes bone formation. We previously reported that CNHs integrated in GBR membranes[19] accelerate bone formation via macrophage activation[20]. The effect of CNHs on bone formation occurred during the early stages of regeneration. However, these results suggest that the specific surface nanostructure of SWCNTs in the membrane exerts different effects on bone formation during the later stages of regeneration. As noted above, part of the HACNT membrane in the tissue was folded (pink arrowhead, Figure 4Ba), and fibrous connective tissue was observed between the membrane and the bone. These findings suggest that the shielding effect of the HACNT membrane could be improved by altering particular mechanical properties, such as increasing the membrane's flexibility. However, selective proliferation of osteoblasts and extensive formation of new bone with the same thickness as the existing bone directly below the membrane were observed *in vitro*, and epithelial cells and fibroblasts did not proliferate on the HACNT membrane culture, whereas osteoblasts proliferated well. These results demonstrate that the HACNT membrane exhibits a sufficient shielding effect to selectively induce the proliferation of osteoblasts, confirming the advantages of using SWCNTs in GBR membranes. Our results thus suggest that the

effect of the specific surface nanostructure of SWCNT membranes in promoting new bone formation opens the possibility of novel applications for these membranes. However, these results should be confirmed by further research.

There is a risk of diffusion of CNTs after they are implanted in the body. Kang et al.[35] reported that CNTs can damage cells through direct contact with the cell membrane. To further investigate the localization and state of SWCNTs in HACNT membranes in this study, resonance Raman mapping of sections of bone tissue was carried out. Figure 5a-cshows different magnifications of histological sections of calvarial bone specimens 8 weeks after HACNT membrane implantation. Figure 5d shows the results of microscopic Raman mapping of the calvarial bone tissue sections. Figure 5e shows the merged image of Figure 3c and 3d. Figure 5d shows a map of the G-band intensity excited at 785 nm overlaid at point 1 (Figure 5f), point 2 (Figure 5g), and point 3 (Figure 5h). Figure 5i shows the intensity at each point, with the intensity of the HACNT membrane portion considered 100%. In the bone tissue adjacent to the HACNT membrane, a small number of SWCNTs were detected (Figure 5d). As shown in Figure S3, the amount of SWCNTs diffusing from the CNT membrane was below the detection limit even after 8 weeks of immersion in phosphate-buffered saline (PBS). The Raman spectral data for SWCNTs around the new bone and the low solubility of HACNTs in PBS suggest that HACNT membranes are highly stable and exhibit very low diffusion of SWCNTs after implantation. Moreover, in our previous study, SWCNTs were implanted between the periosteum and parietal bone in mice. These SWCNTs appeared to be locally stable and did not disperse to other organs[36]. However, further validation of the biocompatibility and low dispersibility

of membranes consisting of SWCNTs is needed.

Conclusions

The HACNT membranes examined in this study exhibited high degrees of strength, hydrophilicity, and stability (insolubility) and promoted selective osteoblast proliferation *in vitro* and formation of new bone in the space created by the membrane. In addition, the membranes exhibited high osteogenic activity *in vivo*. The ability of SWCNTs to absorbing proteins could facilitate further applications and developments, such as loading of growth factors and enhancing membrane toughness and morphologic characteristics. Therefore, SWCNTs could be employed as independent membranes and applied in GBR to promote osteogenesis in cases of significant loss of both the width and volume of alveolar bone due to defects caused by severely advanced periodontal disease, tooth loss, cancer, or accidents. The results of this study represent an important milestone in efforts to create new therapeutic materials for bone regeneration using CNTs.

Experimental section

Preparation of HACNT membranes

SWCNTs (MEIJO eDIPS 1.5p, Japan) were dispersed in 0.1 mg/mL HA (FUJIFILM, Japan) solution at 0.5 mg/mL by bath sonication for 30 min and then homogenized using the following settings: Amp 50%, 1 s/1 s, 10 min, total 20 min. The suspension was then filtered using a membrane filter (Omnipore, 0.1 μm pore, 47 mm diameter) and dried in a 60°C dry oven. The HACNT membranes were stripped from the filter membranes and then treated for hydrophilicity using a UV ozone cleaner (PC450, Meiwa fosis, Japan) for 10 min.

Characterization of HACNT membranes

HACNT membranes were observed by SEM at 10 kV (SEM, S-400, Hitachi, Tokyo, Japan). The CA was measured using a Phoenix Alpha P200 instrument (Meiwa fosis, Japan). For mechanical strength testing, a dumb-bell shape SWCNT membrane was fabricated with 2 mm width in the middle and stretched using an MST-I type HS/HR (Shimadzu, Japan) with a 25 N load cell; PTFE membranes were also analyzed using the same method for comparison. The membrane thickness was measured using a constant-pressure thickness gauge (PG-02, TECLOCK, Japan).

In vitro experiments

Cell culture

Mouse calvaria osteoblastic cells (MC3T3-E1)[37] and human gingival carcinoma epithelial-like cells (Ca9-22)[38] were cultured in Minimum Essential Medium Eagle (Sigma-Aldrich, St. Louis, MO, USA) containing 10% fetal bovine serum (CELLECT, France), 2 mM glutamine, and 1% penicillin/streptomycin (Thermo Fisher Scientific, Gibco, Waltham, MA) at 50 U/mL penicillin and 50 mg/mL streptomycin. Mouse embryonic fibroblasts cells (NIH/3T3)[39] were cultured in Dulbecco's Modified Eagle's Medium-high glucose (Sigma-Aldrich) containing 10% calf serum (Funakoshi, Japan) and 1% penicillin/streptomycin (Thermo Fisher Scientific, Gibco) at 50 U/mL penicillin and 50 mg/mL streptomycin. All cells were cultured at 37°C in a 5% CO_2 atmosphere.

To evaluate the proliferation of each cell type on HACNT membranes, membranes were placed at the bottom of wells in a 48-well plate (Corning, Kennebunk, ME, USA), and 500 μL of a suspension of each cell type at 2 $\times 10^4$ cells/mL was seeded in wells with the HACNT membranes or blank wells as controls and incubated for 3 and 7 days.

SEM observation

After 3 days, cells on the HACNT membranes were observed by SEM. Prior to analysis, the cells adhering to the membranes were washed three times with PBS and fixed with 2.5% glutaraldehyde. After dehydration through a graded ethanol series, the cells were dried using the critical point method and sputter coated with palladium-platinum for SEM observation.

Quantification of DNA content

After 3 and 7 days of cultivation, the wells and HACNT membranes were washed with PBS, and 300 μL of 0.2% IGEPAL CA630 (Sigma-Aldrich) was added to each well. The cell samples were then frozen, thawed, and homogenized. To each of the resulting cell lysates was added 100 mL of 4 M NaCl/0.1 M phosphate buffer (pH 7.4), and the samples were centrifuged for DNA analysis. Picogreen (Thermo Fischer Scientific) was used to measure the DNA content via a fluorometer (Infinite F200 PRO, Tecan, Switzerland), with the excitation filter set at 356 nm and the emission filter at 458 nm.

Animal experiments

To investigate new bone regeneration ability and safety of HACNT membranes, Wistar rats with calvarial defects were used as an animal model. All animal experiments were approved and performed in accordance with the regulations of the Animal Care and Use Committee of Hokkaido University (no. 19-0061).

Bone regeneration evaluation

Ten-week-old male Wistar rats (approx. 300 g; CLEA Japan Inc., Tokyo, Japan) were anesthetized using inhaled isoflurane (Pfizer Inc., New York, NY, USA), after which the hair around the calvarial region was shaved and the skin sterilized with 70% ethanol. A semicircular incision was made on the scalp, and the skin and periosteum were separated, exposing the calvarial bone by blunt dissection. An 8-mm diameter bone defect was

made on the exposed calvarial bone using a 7/8-mm diameter trephine bur (Stoma, Germany). The defect was either covered with a 12-mm diameter HACNT membrane or left untreated as a control (n=6). After 8 weeks, rats were anesthetized with inhaled isoflurane and perfusion fixed using fixation solution (2.5% glutaraldehyde with 0.1 M HEPES).

Samples of calvarial bone and membranes were harvested and fixed in fixation solution. For radiographic evaluation, the samples were scanned using μ-CT, (CosmoScan, Rigaku). The acquired CT images were imported into Fuji ImageJ software, and the 3D script plugin was used to 3D reconstruct and evaluate the samples. Materialize Mimics version 21.0 software was also used to calculate the volume of new bone formed in the defect area[40], and the bone volume in the surgically made defect area was calculated as new regenerated bone volume. For subsequent histological evaluation, the samples were embedded in resin, sliced into 30- to 40-μm sections in the coronal plane, stained with toluidine blue, and observed under an optical microscope.

Statistical analysis

Differences in bone volume between each group were analyzed using the Mann-Whitney test. Differences in DNA content on the membrane were examined using two-way analysis of variance with Sidak's correction. Statistical significance was established at $P < 0.05$.

Raman imaging

Micro-Raman mapping was carried out using a Renishaw inVia confocal microscope equipped with a 785-nm laser excitation source, as previously reported[41]. The laser, attenuated to approximately 0.5 mW, was focused on the sample surface with a 50× objective lens with an NA of 0.75. The spot size was estimated to be approximately 0.87 μm. This size mainly determines the spatial resolution of the Raman images. Raman signals from the sample were measured using an electron-multiplying charge-coupled device (CCD) detector (Andor) through a grating with 1200 grooves/mm. The step size of the measurements was 1.0 μm. The CCD integration time was 0.05 s for all measurements. The resulting Raman spectra were fitted using the Lorenz function, and Raman images were obtained by plotting the peak area intensities of the fitting results.

Figures

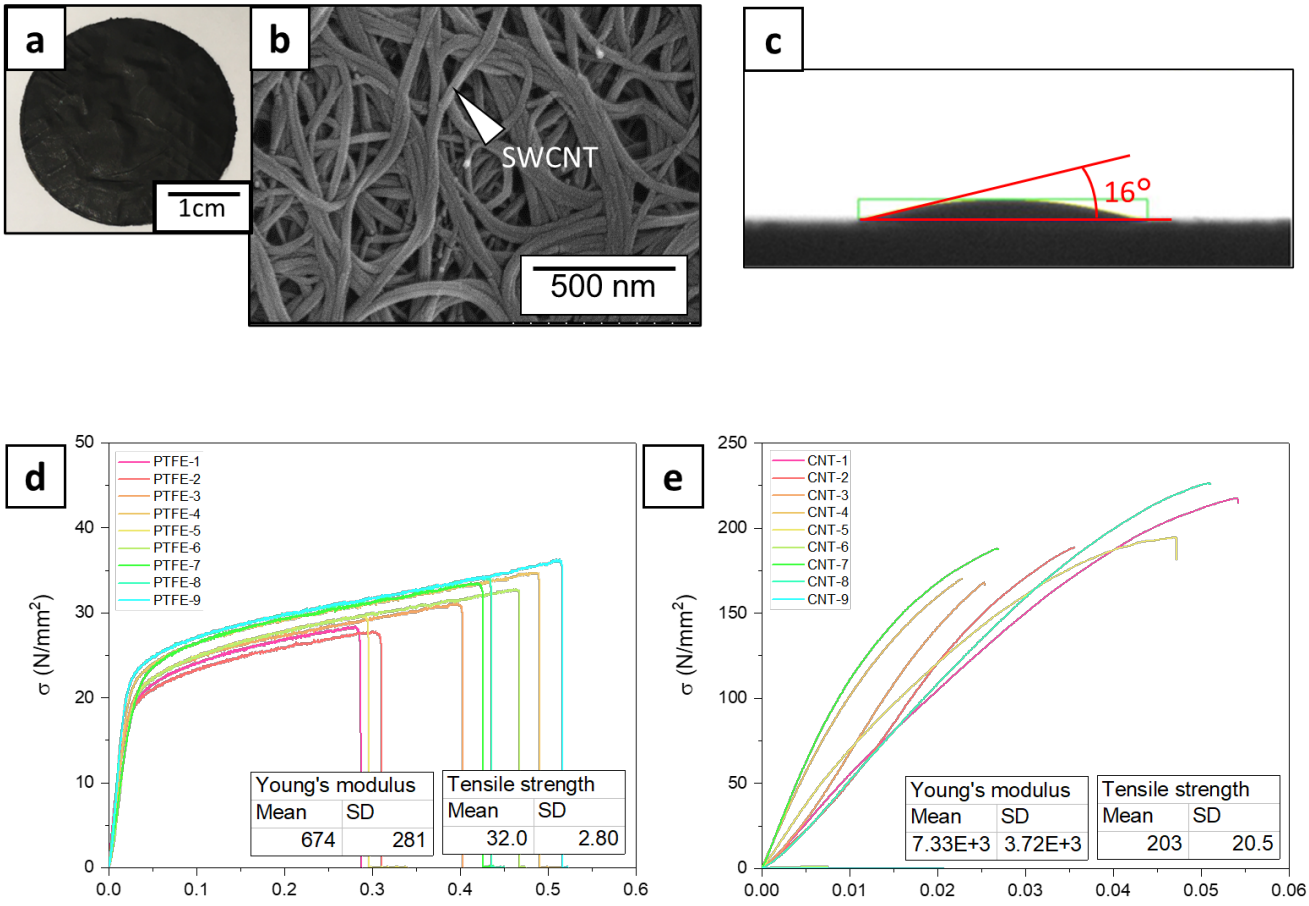

Figure 1. Characterization of HACNT membranes. (a) Photograph of an HACNT membrane. (b) SEM image of an HACNT membrane; the membrane consists of many bundles of SWCNTs (arrowhead). (c) Image of the spreading of a water drop on an HACNT membrane. Average CA was approximately 16°. Graph of tensile strength of (d) PTFE membrane and (e) HACNT membrane. Mean tensile strength: PTFE membrane=32 N/mm², HACNT membrane: 203 N/mm². Mean Young's modulus: PTFE membrane=674 N/mm², HACNT membrane: 7330 N/mm²(n=9)

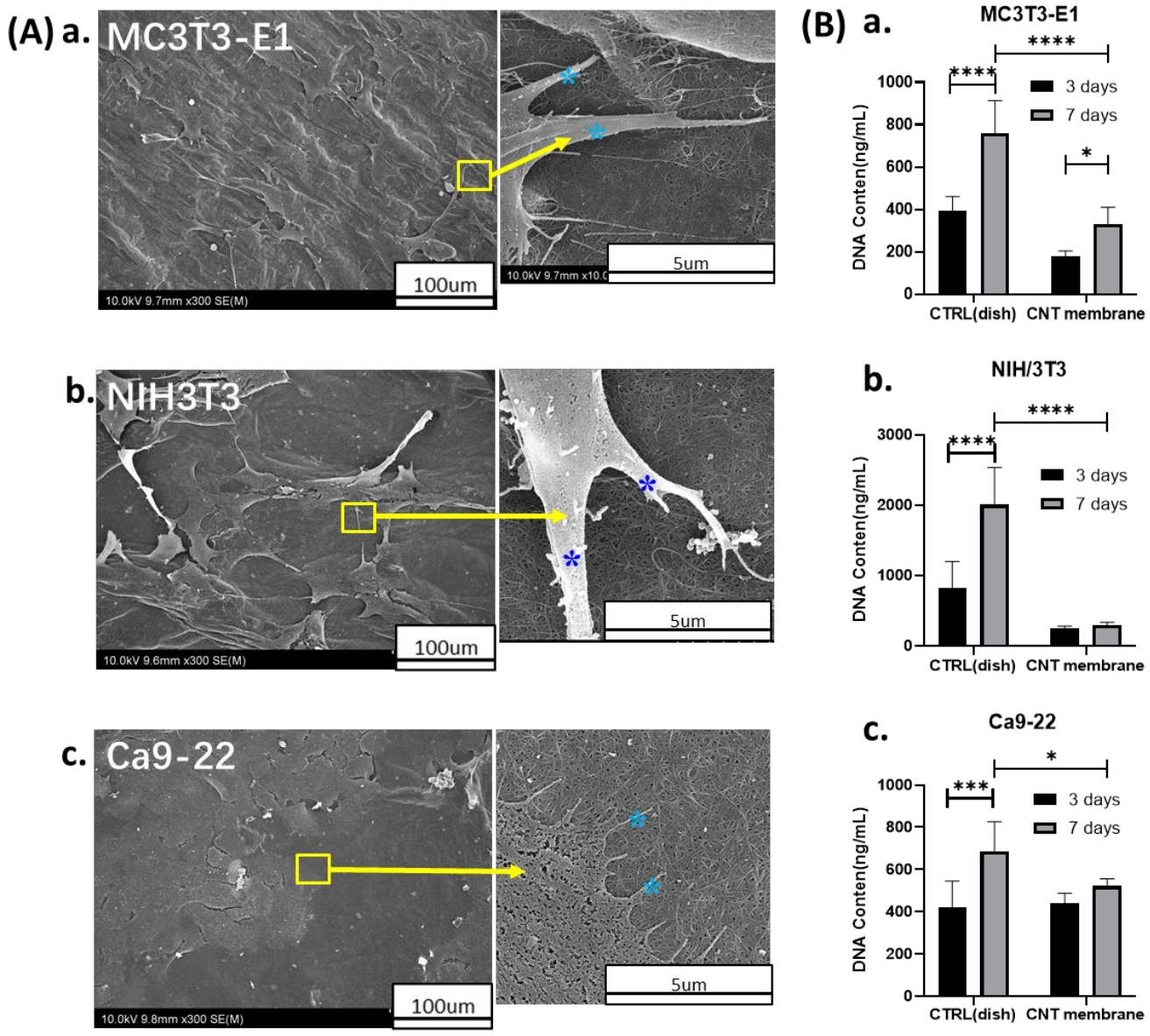

Figure 2. (A) SEM observations of MC3T3-E1 (a), NIH3T3 (b), and Ca9-22 (c) cells cultured on HACNT membranes for 3 days (pseudopodia: blue asterisks). (B) DNA content of MC3T3-E1 (a), NIH3T3 (b), and Ca9-22 (c) cells on HACNT membranes after 3 and 7 days of culture (n=6, **P*<0.05, ****P*<0.001, *****P*<0.0001).

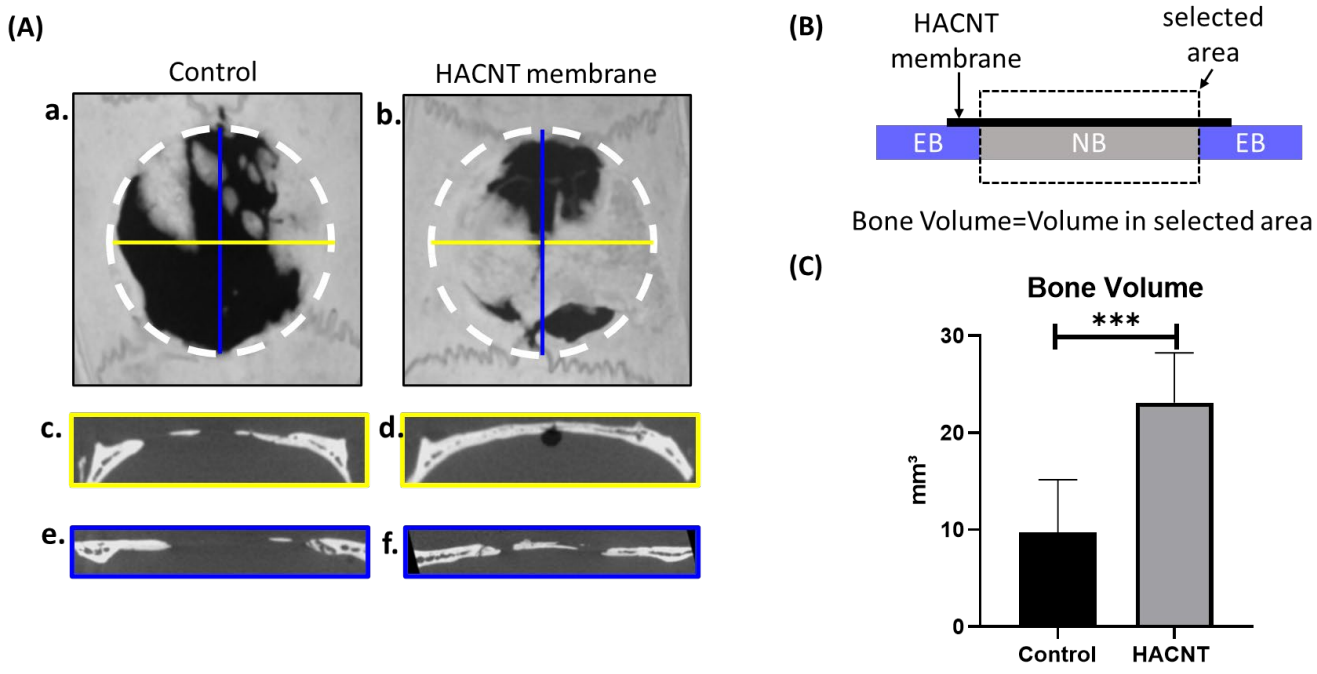

Figure 3. (A) Micro-CT images of representative rat calvarial bone samples with/without HACNT implantation after 8 weeks. (a, c, e) Control (without membrane) and (b, d, f) HACNT membrane groups were observed in 3 planes of direction: (a, b) horizontal plane; (c, d) coronal plane; (e, f) sagittal plane. (B) Schematic illustration of the method to measure bone volume; new bone was defined as the volume in the selected area. EB: existing bone. NB: new bone. (C) Comparison of volume of new bone regenerated in the calvarial bone defect area of the two groups (n=6, ***P<0.001).

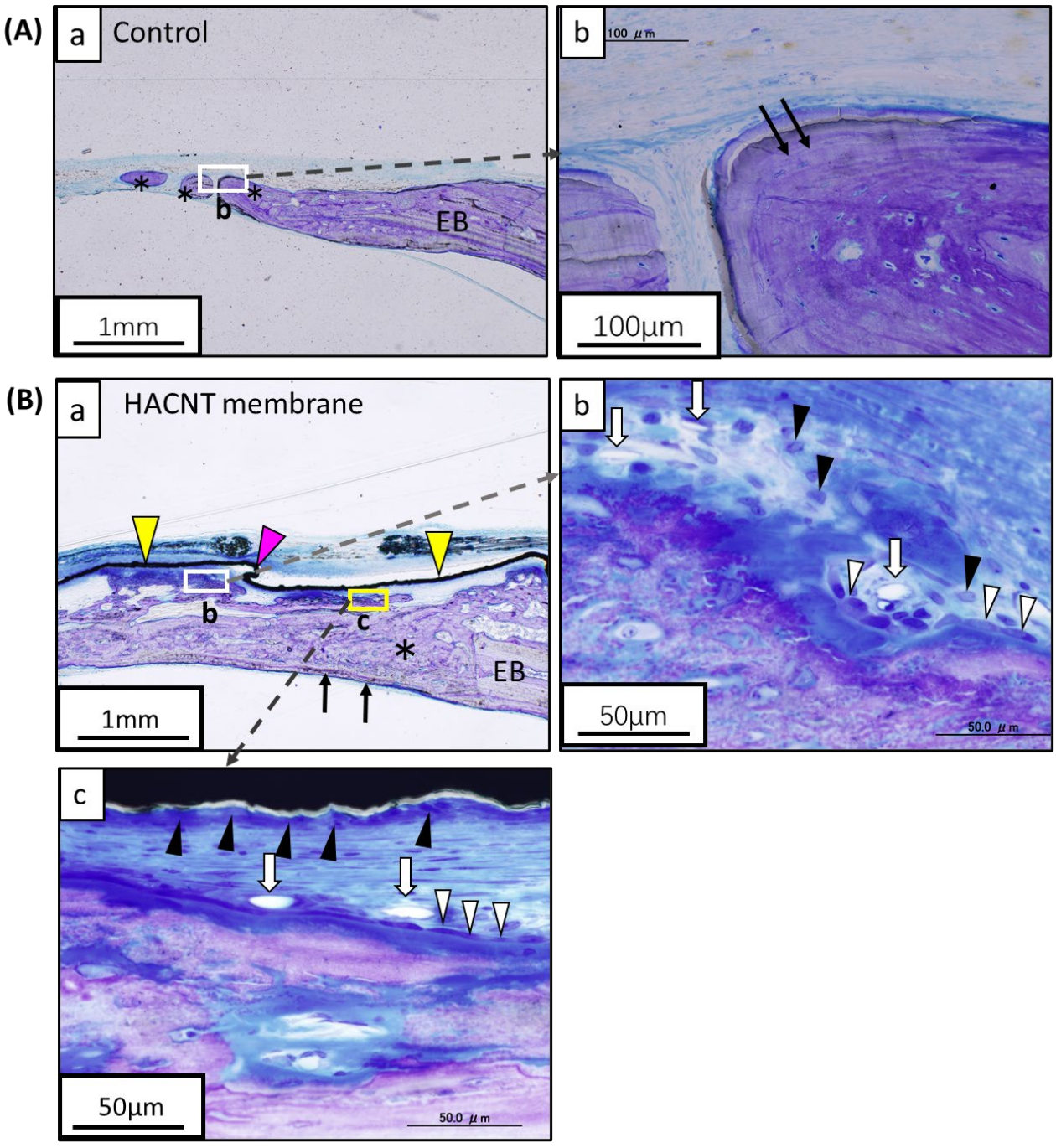

Figure 4. Representative histological sections of rat calvarial bone with/without HACNT implantation after 8 weeks. (A) Without membrane (control). (a) Thick fibrous connective tissue covered the bone defect. New bone (black asterisks) was formed in the defect. (b) High magnification of white square in (Aa). Lamellar structures

(black arrows) were seen. (B) With HACNT membrane. (a) HACNT membrane (yellow arrowheads) covered newly formed bone (*) and existing bone (EB). A portion of membrane was folded (pink arrowhead). (b) High magnification of white square in (Ba). Active osteogenesis was seen in the upper part of the newly formed bone. Osteoblasts (white arrowheads) and large cells, such as mesenchymal cells (black arrowheads), were observed in new bone. (c) High magnification of yellow square of (Ba). Many large cells such as mesenchymal cells (black arrowheads) were observed close to the CNT membrane. Osteoblasts (white arrowheads) and capillaries (white arrows) indicating active osteogenesis were observed.

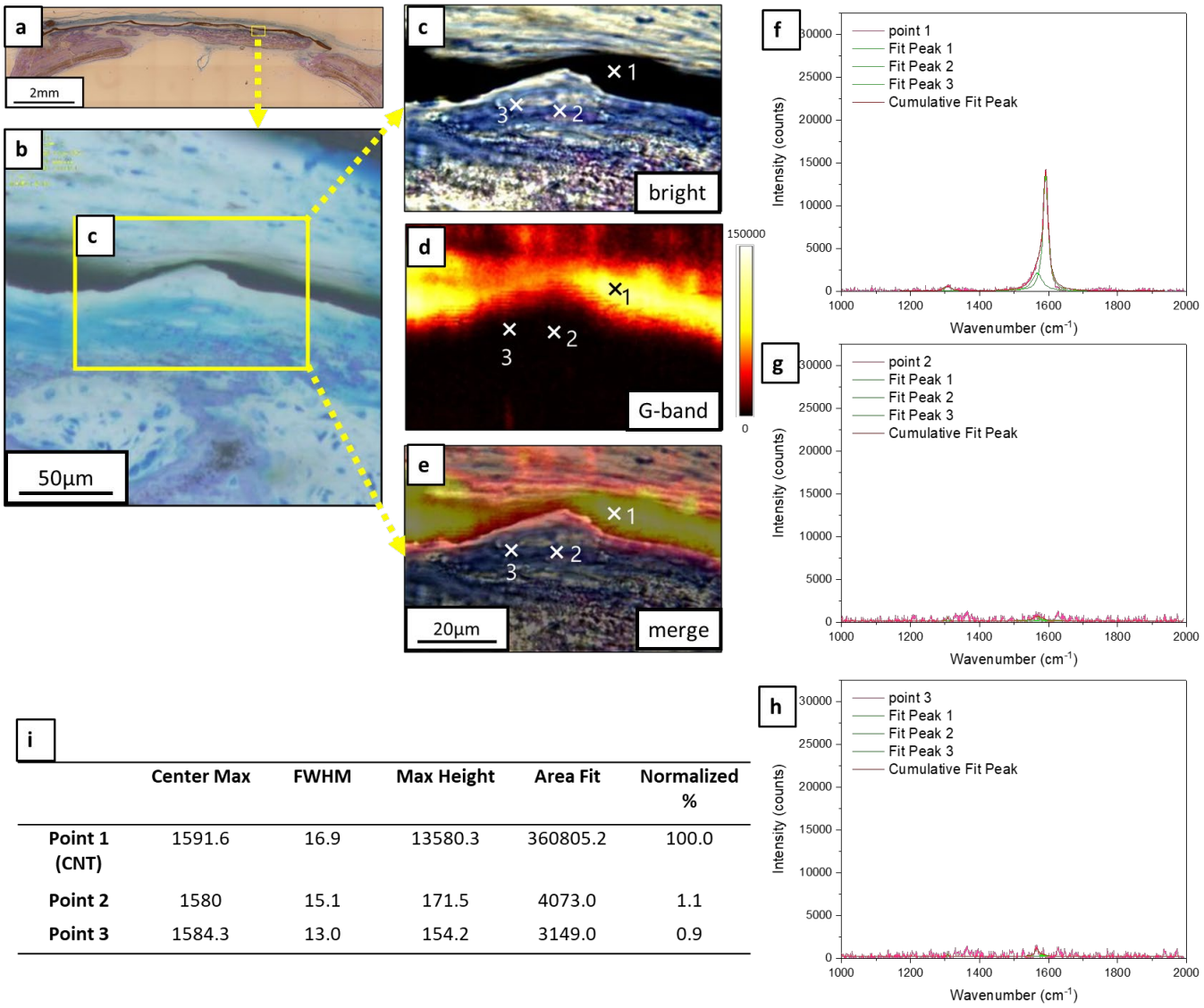

i

	Center Max	FWHM	Max Height	Area Fit	Normalized %
Point 1 (CNT)	1591.6	16.9	13580.3	360805.2	100.0
Point 2	1580	15.1	171.5	4073.0	1.1
Point 3	1584.3	13.0	154.2	3149.0	0.9

Figure 5. (a) Histological sections of calvarial bone specimens implanted with HACNT membranes after 8 weeks. (b) High magnification of (a). (c-e) Raman imaging at high magnification of yellow square in (b). (c) Bright field, (d) G-band field, and (e) merge field under Raman microscopy observation; three points were selected to observe CNTs ("×" were detection point). Graphs (f- h) show intensity spectra of excitation at 785 nm at the three points;

intensity of CNTs was normalized to 100%. (f) Point 1 (CNT): 100%. (g) Point 2: 1.1%. (h) Point 3: 0.9%. Table (i) shows the intensity of each point.

Author Information

Corresponding author

Tel: +81-11-706-4270 Fax: +81-11-706-4903

E-mail address: erieri@den.hokudai.ac.jp* (E. Hirata)

ORCID id: 0000-0001-6718-1465

Funding Sources

This study was supported by a KAKENHI Grant-in-Aid for Scientific Research C (ID No. 20K10025 to E. H.) and a KAKENHI Grant-in-Aid for Scientific Research B (ID No. 19H03839 to A. Y.).

Acknowledgments

We thank Dr. Kousuke Nakamura, Faculty of Science Hokkaido University, for preparing thin sections from the samples.

Supporting Information.

Absorbance of filtering solution of HACNT membrane comparing with 0.1mg/mL HA solution.

DNA content and ALP activity of mouse bone marrow stromal cells (mBMCs) culture in the medium with 0.05, 0.1. 0.5 mg/mL hyaluronic acid solution. Absorbance of PBS solution with HACNT membrane immersed after 8

weeks at room temperature and pressure. SEM observations of MC3T3-E1, NIH3T3 and Ca9-22 cells cultured on HACNT membrane after 4 and 24 hours. PTFE membrane implantation on rat calvarial bone defect for 8 weeks

References

(1) Iijima, S. Helical microtubules of graphitic carbon. *Nature* **1991**, *354* (6348), 56–58 DOI: 10.1038/354056a0.

(2) Iijima, S.; Ichihashi, T. Single-shell carbon nanotubes of 1-nm diameter. *Nature* **1993**, *363* (6430), 603–605 DOI: 10.1038/363603a0.

(3) Liu, X.; George, M. N.; Park, S.; Miller II, A. L.; Gaihre, B.; Li, L.; Waletzki, B. E.; Terzic, A.; Yaszemski, M. J.; Lu, L. 3D-printed scaffolds with carbon nanotubes for bone tissue engineering: Fast and homogeneous one-step functionalization. *Acta Biomater.* **2020**, *111*, 129–140 DOI: 10.1016/j.actbio.2020.04.047.

(4) Patel, K. D.; Kim, T. H.; Mandakhbayar, N.; Singh, R. K.; Jang, J. H.; Lee, J. H.; Kim, H. W. Coating biopolymer nanofibers with carbon nanotubes accelerates tissue healing and bone regeneration through orchestrated cell- and tissue-regulatory responses. *Acta Biomater.* **2020**, *108*, 97–110 DOI: 10.1016/j.actbio.2020.03.012.

(5) Peng, Z.; Zhao, T.; Zhou, Y.; Li, S.; Li, J.; Leblanc, R. M. Bone Tissue Engineering via Carbon-Based Nanomaterials. *Adv. Healthc. Mater.* **2020**, *9* (5), 1–30 DOI: 10.1002/adhm.201901495.

(6) Huang, B.; Vyas, C.; Byun, J. J.; El-Newehy, M.; Huang, Z.; Bártolo, P. Aligned multi-walled carbon nanotubes with nanohydroxyapatite in a 3D printed polycaprolactone scaffold stimulates osteogenic differentiation. *Mater. Sci. Eng. C* **2020**, *108* (July 2019), 110374 DOI: 10.1016/j.msec.2019.110374.

(7) Genady, A. R.; Fong, D.; Slikboer, S. R.; El-Zaria, M. E.; Swann, R.; Janzen, N.; Faraday, A.; McNelles, S. A.; Rezvani, M.; Sadeghi, S.; et al. 99mTc-Functionalized Single-Walled Carbon Nanotubes for Bone Targeting. *ACS Appl. Nano Mater.* **2020**, *3* (12), 11819–11824 DOI: 10.1021/acsanm.0c02339.

(8) Usui, Y.; Aoki, K.; Narita, N.; Murakami, N.; Nakamura, I.; Nakamura, K.; Ishigaki, N.; Yamazaki, H.; Horiuchi, H.; Kato, H.; et al. Carbon nanotubes with high bone-tissue compatibility and bone-formation acceleration effects. *Small* **2008**, *4* (2), 240–246 DOI: 10.1002/smll.200700670.

(9) Barrientos-Durán, A.; Carpenter, E. M.; Zur Nieden, N. I.; Malinin, T. I.; Rodríguez-Manzaneque, J. C. arlo.; Zanello, L. P. Carboxyl-modified single-wall carbon nanotubes improve bone tissue formation in vitro and repair in an in vivo rat model. *Int. J. Nanomedicine* **2014**, *9*, 4277–4291 DOI: 10.2147/IJN.S62538.

(10) Hirata, E.; Uo, M.; Takita, H.; Akasaka, T.; Watari, F.; Yokoyama, A. Multiwalled carbon nanotube-coating of 3D collagen scaffolds for bone tissue engineering. *Carbon* **2011**, *49* (10), 3284–3291 DOI: 10.1016/j.carbon.2011.04.002.

(11) Hirata, E.; Uo, M.; Nodasaka, Y.; Takita, H.; Ushijima, N.; Akasaka, T.; Watari, F.; Yokoyama, A. 3D collagen scaffolds coated with multiwalled carbon nanotubes: Initial cell attachment to internal surface. *J. Biomed. Mater. Res. - Part B Appl. Biomater.* **2010**, *93* (2), 544–550 DOI: 10.1002/jbm.b.31613.

(12) Hirata, E.; Uo, M.; Takita, H.; Akasaka, T.; Watari, F.; Yokoyama, A. Development of a 3D collagen scaffold coated with multiwalled carbon nanotubes. *J. Biomed. Mater. Res. - Part B Appl. Biomater.* **2009**,

90 B (2), 629–634 DOI: 10.1002/jbm.b.31327.

(13) Hirata, E.; Ménard-Moyon, C.; Venturelli, E.; Takita, H.; Watari, F.; Bianco, A.; Yokoyama, A. Carbon nanotubes functionalized with fibroblast growth factor accelerate proliferation of bone marrow-derived stromal cells and bone formation. *Nanotechnology* **2013**, *24* (43), 435101 DOI: 10.1088/0957-4484/24/43/435101.

(14) Omar, O.; Elgali, I.; Dahlin, C.; Thomsen, P. Barrier membranes: More than the barrier effect? *J. Clin. Periodontol.* **2019**, *46* (S21), 103–123 DOI: 10.1111/jcpe.13068.

(15) Dahlin, C.; Linde, A.; Gottlow, J.; Nyman, S. Healing of Bone Defects by Guided Tissue Regeneration. *Plast. Reconstr. Surg.* **1988**, *81* (5), 672–676 DOI: 10.1097/00006534-198805000-00004.

(16) Hämmerle, C. H. F.; Jung, R. E. Bone augmentation by means of barrier membranes. *Periodontol. 2000* **2003**, *33*, 36–53 DOI: 10.1046/j.0906-6713.2003.03304.x.

(17) Elgali, I.; Omar, O.; Dahlin, C.; Thomsen, P. Guided bone regeneration: materials and biological mechanisms revisited. *Eur. J. Oral Sci.* **2017**, *125* (5), 315–337 DOI: 10.1111/eos.12364.

(18) Kim, H. Y.; Park, J. H.; Byun, J. H.; Lee, J. H.; Oh, S. H. BMP-2-Immobilized Porous Matrix with Leaf-Stacked Structure as a Bioactive GBR Membrane. *ACS Appl. Mater. Interfaces* **2018**, *10* (36), 30115–30124 DOI: 10.1021/acsami.8b09558.

(19) Kasai, T.; Matsumura, S.; Iizuka, T.; Shiba, K.; Kanamori, T.; Yudasaka, M.; Iijima, S.; Yokoyama, A. Carbon nanohorns accelerate bone regeneration in rat calvarial bone defect. *Nanotechnology* **2011**, *22* (6),

065102 DOI: 10.1088/0957-4484/22/6/065102.

(20) Hirata, E.; Miyako, E.; Hanagata, N.; Ushijima, N.; Sakaguchi, N.; Russier, J.; Yudasaka, M.; Iijima, S.; Bianco, A.; Yokoyama, A. Carbon nanohorns allow acceleration of osteoblast differentiation via macrophage activation. *Nanoscale* **2016**, *8* (30), 14514–14522 DOI: 10.1039/C6NR02756C.

(21) Iijima, S. Carbon nanotubes: Past, present, and future. *Phys. B Condens. Matter* **2002**, *323* (1–4), 1–5 DOI: 10.1016/S0921-4526(02)00869-4.

(22) Newman, P.; Minett, A.; Ellis-Behnke, R.; Zreiqat, H. Carbon nanotubes: Their potential and pitfalls for bone tissue regeneration and engineering. *Nanomedicine Nanotechnology, Biol. Med.* **2013**, *9* (8), 1139–1158 DOI: 10.1016/j.nano.2013.06.001.

(23) Zhang, J.; Li, J.; Han, Y. Superhydrophobic PTFE surfaces by extension. *Macromol. Rapid Commun.* **2004**, *25* (11), 1105–1108 DOI: 10.1002/marc.200400065.

(24) Padial-Molina, M.; Galindo-Moreno, P.; Fernández-Barbero, J. E.; O'Valle, F.; Jódar-Reyes, A. B.; Ortega-Vinuesa, J. L.; Ramón-Torregrosa, P. J. Role of wettability and nanoroughness on interactions between osteoblast and modified silicon surfaces. *Acta Biomater.* **2011**, *7* (2), 771–778 DOI: 10.1016/j.actbio.2010.08.024.

(25) Toffoli, A.; Parisi, L.; Bianchi, M. G.; Lumetti, S.; Bussolati, O.; Macaluso, G. M. Thermal treatment to increase titanium wettability induces selective proteins adsorption from blood serum thus affecting osteoblasts adhesion. *Mater. Sci. Eng. C* **2020**, *107* (August 2019) DOI: 10.1016/j.msec.2019.110250.

(26) van Kooten, T. G.; Schakenraad, J. M.; van der Mei, H. C.; Busscher, H. J. Influence of substratum wettability on the strength of adhesion of human fibroblasts. *Biomaterials* **1992**, *13* (13), 897–904 DOI: 10.1016/0142-9612(92)90112-2.

(27) Foraida, Z. I.; Kamaldinov, T.; Nelson, D. A.; Larsen, M.; Castracane, J. Elastin-PLGA hybrid electrospun nanofiber scaffolds for salivary epithelial cell self-organization and polarization. *Acta Biomater.* **2017**, *62*, 116–127 DOI: 10.1016/j.actbio.2017.08.009.

(28) Ribeiro, N.; Sousa, S. R.; Monteiro, F. J. Influence of crystallite size of nanophased hydroxyapatite on fibronectin and osteonectin adsorption and on MC3T3-E1 osteoblast adhesion and morphology. *J. Colloid Interface Sci.* **2010**, *351* (2), 398–406 DOI: 10.1016/j.jcis.2010.08.013.

(29) Aoyagi, A.; Hata, M.; Matsukawa, R.; Imanishi, Y.; Takebe, J. Physicochemical properties of anodized-hydrothermally treated titanium with a nanotopographic surface structure promote osteogenic differentiation in dental pulp stem cells. *J. Prosthodont. Res.* **2021**, *65* (4), 474–481 DOI: 10.2186/jpr.jpr_d_20_00114.

(30) Kunzler, T. P.; Drobek, T.; Schuler, M.; Spencer, N. D. Systematic study of osteoblast and fibroblast response to roughness by means of surface-morphology gradients. *Biomaterials* **2007**, *28* (13), 2175–2182 DOI: 10.1016/j.biomaterials.2007.01.019.

(31) Baharloo, B.; Textor, M.; Brunette, D. M. Substratum roughness alters the growth, area, and focal adhesions of epithelial cells, and their proximity to titanium surfaces. *J. Biomed. Mater. Res. - Part A* **2005**,

74 (1), 12–22 DOI: 10.1002/jbm.a.30321.

(32) Hemshekhar, M.; Thushara, R. M.; Chandranayaka, S.; Sherman, L. S.; Kemparaju, K.; Girish, K. S. Emerging roles of hyaluronic acid bioscaffolds in tissue engineering and regenerative medicine. *Int. J. Biol. Macromol.* **2016**, *86*, 917–928 DOI: 10.1016/j.ijbiomac.2016.02.032.

(33) Schanté, C. E.; Zuber, G.; Herlin, C.; Vandamme, T. F. Chemical modifications of hyaluronic acid for the synthesis of derivatives for a broad range of biomedical applications. *Carbohydr. Polym.* **2011**, *85* (3), 469–489 DOI: 10.1016/j.carbpol.2011.03.019.

(34) Silva, C. R.; Babo, P. S.; Gulino, M.; Costa, L.; Oliveira, J. M.; Silva-Correia, J.; Domingues, R. M. A.; Reis, R. L.; Gomes, M. E. Injectable and tunable hyaluronic acid hydrogels releasing chemotactic and angiogenic growth factors for endodontic regeneration. *Acta Biomater.* **2018**, *77*, 155–171 DOI: 10.1016/j.actbio.2018.07.035.

(35) Kang, S.; Herzberg, M.; Rodrigues, D. F.; Elimelech, M. Antibacterial effects of carbon nanotubes: Size does matter! *Langmuir* **2008**, *24* (13), 6409–6413 DOI: 10.1021/la800951v.

(36) Hirata, E.; Yudasaka, M.; Ushijima, N.; Sakaguchi, N.; Maeda, Y.; Tanaka, T.; Kataura, H.; Yokoyama, A. Fate of Carbon Nanotubes Locally Implanted in Mice Evaluated by Near-Infrared Fluorescence Imaging: Implications for Tissue Regeneration. *ACS Appl. Nano Mater.* **2019**, *2* (3), 1382–1390 DOI: 10.1021/acsanm.8b02267.

(37) Kodama, H.; Amagai, Y.; Sudo, H.; Kasai, S.; Yamamoto, S. Establishment of a clonal osteogenic cell line

from newborn mouse calvaria. *Japanese J. Oral Biol.* **1981**, *23* (4), 899–901 DOI: 10.2330/joralbiosci1965.23.899.

(38) Kaga, N.; Akasaka, T.; Matsuura, T.; Yokoyama, A.; Yoshida, Y. Proliferation of Saos-2 and Ca9-22 cells on grooved and pillared titanium surfaces. *Biomed. Mater. Eng.* **2020**, *30* (5–6), 559–567 DOI: 10.3233/BME-191074.

(39) TODARO, G. J.; GREEN, H. Quantitative studies of the growth of mouse embryo cells in culture and their development into established lines. *J. Cell Biol.* **1963**, *17* (6), 299–313 DOI: 10.1083/jcb.17.2.299.

(40) Perez, M.; Fornell, P.; Garcia-Aznar, J.; Doblaré, M. Validation of bone remodelling models applied to different bone types using Mimics. **2007**, No. January 2016.

(41) Takeuchi, T.; Iizumi, Y.; Yudasaka, M.; Kizaka-Kondoh, S.; Okazaki, T. Characterization and biodistribution analysis of oxygen-doped single-walled carbon nanotubes used as in vivo fluorescence imaging probes. *Bioconjug. Chem.* **2019**, *30* (5), 1323–1330 DOI: 10.1021/acs.bioconjchem.9b00088.

For Table of Contents Use Only

(Graphical abstract)

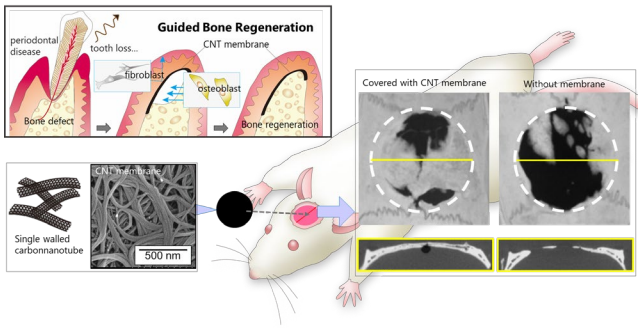

Single-walled Carbon Nanotube Membranes Accelerate Active Osteogenesis in Bone Defects: Potential of Guided Bone Regeneration Membranes

Yikun Xu,[†] Eri Hirata,[†] Yoko Iizumi,[§] Natsumi Ushijima,[†] Keisuke Kubota,[†] Sadahito Kimura,[†]*

Yukari Maeda,[†] Toshiya Okazaki,[§] and Atsuro Yokoyama[†]

[†] Graduate School of Dental Medicine, Hokkaido University, Sapporo 060-8586, Japan

[§] Nanomaterials Research Institute (NMRI), National Institute of Advanced Industrial Science and Technology (AIST), Tsukuba Central, Tsukuba 305-8565, Japan

Supporting information

Single-walled Carbon Nanotube Membranes Accelerate Active Osteogenesis in Bone Defects: Potential of Guided Bone Regeneration Membranes

Yikun Xu,† Eri Hirata,† Yoko Iizumi,§ Natsumi Ushijima,† Keisuke Kubota,† Sadahito Kimura,† Yukari Maeda,† Toshiya Okazaki,§ and Atsuro Yokoyama†*

†Graduate School of Dental Medicine, Hokkaido University, Sapporo 060-8586, Japan

§Nanomaterials Research Institute (NMRI), National Institute of Advanced Industrial Science and Technology (AIST), Tsukuba Central, Tsukuba 305-8565 Japan

Corresponding author. Tel: +81-11-706-4270 Fax: +81-11-706-4903

E-mail address: erieri@den.hokudai.ac.jp *(E. Hirata)

Pages: 7

Figures: 5

Contents

Figure S1: Absorbance of filtering solution of HACNT membrane comparing with 0.1mg/mL HA solution.

Figure S2: DNA content and ALP activity of mouse bone marrow stromal cells (mBMCs) culture in the medium with 0.05, 0.1. 0.5 mg/mL hyaluronic acid solution.

Figure S3: Absorbance of PBS solution with HACNT membrane immersed after 8 weeks at room temperature and pressure.

Figure S4. SEM observations of MC3T3-E1, NIH3T3 and Ca9-22 cells cultured on HACNT membrane after 4 and 24 hours. Asterisk: cell. Triangle: HACNT membrane.

Figure S5. (A) Micro-CT images of representative rat's calvarial bone samples with PTFE membrane implantation after 8 weeks. (a): horizontal plane. (b): coronal plane. (c): sagittal plane . (B) Representative histological sections of rat PTFE implantation after 8 weeks. (a) Thin bone tissue was formed from existing bone (EB) under PTFE membrane (yellow arrowhead). (b) Some part of new bone with osteocytes (yellow arrow) were attached to PTFE membrane (yellow arrowhead) directly. Lamellar structure (asterisk) that indicated stable bone remodeling was observed lower part of newly formed bone.

Supporting materials and methods

Measurement of elution of HACNT membranes into PBS

1.0 mg of HACNT membranes were immersed in 10 ml of PBS and allowed to stand for 8 weeks at room temperature and pressure. 10 ml of PBS without CNTs was used as a control. 5 ml of the PBS solution after removing the CNT membranes was dispensed into a separate vial, 50 mg of SDBS was added, and the solution was dispersed by bath sonication for 30 min. The absorption spectra of both sample and control groups were measured by optical absorption spectrometer (UV-3100, Shimadzu, Japan) and compared.

Quantifying the volume of hyaluronic acid in the HACNT membrane

The amount of hyaluronic acid contained in HACNT membrane was calculated form the concentration of hyaluronic acid in the filtrated solution. Absorption spectrum of both the filtrated solution and 0.1mg/ml hyaluronic acid were measured by optical absorption spectrometer and compared.

Cell proliferation and differentiation by changing HLA concentration

Mouse bone marrow stromal cells (mBMSCs, ATCC) were cultured in Dulbecco's Modified Eagle's Medium-high glucose (Sigma-Aldrich, St. Louis, MO, USA) containing 10% fetal bovine serum (Funakoshi, Japan) and 1% penicillin/streptomycin (Thermo Fischer Scientific, Gibco, Waltham, MA) at 50 U/mL penicillin and 50 mg/mL streptomycin. All cells were cultured at 37℃ with a 5% CO2 atmosphere.

For evaluation of each cell's proliferation and ALP activity in different concentrations of hyaluronic acid solution. Cells were suspended in 500 μL culture medium with 0, 0.05, 0.1, 0.5mg/mL hyaluronic acid solution and seeded in a density of 1 $\times 10^4$ cells/mL in 48-well-plate (Corning, Kennebunk, ME, USA) for 7 days.

After 7 days of cultivation, the wells were washed with PBS. 300 μL of the 0.2% IGEPAL CA630 (Sigma-Aldrich, MO, USA) was added to each well. The samples were frozen, thawed, and then homogenized. The sample solution was added to 100 μL of 4M NaCl, 0.1M phosphate buffer (pH 7.4), and then centrifuged for DNA analysis. Picogreen (Thermo Fischer Scientific, Waltham, MA) was used to measure the DNA content via a fluorometer (Infinite F200 PRO, Tecan, Switzerland) with the excitation filter set at 356nm and the emission filter at 458 nm.

Alkaline phosphatase (ALP) activity was measured with LabAssay (Wako, Japan). Twenty microliters of the supernatant fluid in the sample were added to 100 μL of p-nitrophenol phosphate in carbonate buffer and incubated for 15 min at 37°C. After 80 μL of NaOH was added, absorbance was measured at 405 nm using the fluorometer (Infinite F200 PRO, Tecan, Switzerland) and enzyme activity was determined from the calibration curve p-nitrophenol standard. ALP activity was normalized by DNA content (n=5).

DNA content and ALP activity were analyzed by a two-way ANOVA test and sidak's correction. Statistical significance was established at $P < 0.05$.

Cell culturing

Mouse calvaria osteoblastic cells (MC3T3-E1), human gingival carcinoma epithelial-like cells (Ca9-22)

Mouse embryonic fibroblasts cells (NIH/3T3) were cultured. To evaluate the proliferation of each cell type on HACNT membranes, 500 μL of a suspension of each cell type at 2×10^5 cells/mL was seeded in wells with the HACNT membranes incubated. After 4 and 24 hours, cells on the HACNT membranes were observed by SEM.

Animal experiments

To compare bone regeneration ability of HACNT membranes, the PTFE membrane were implanted in Wistar rats calvarial defects with same surgical procedure, and the samples were also evaluated by μ-CT and embedded in resin for histological evaluation.

Supporting figures

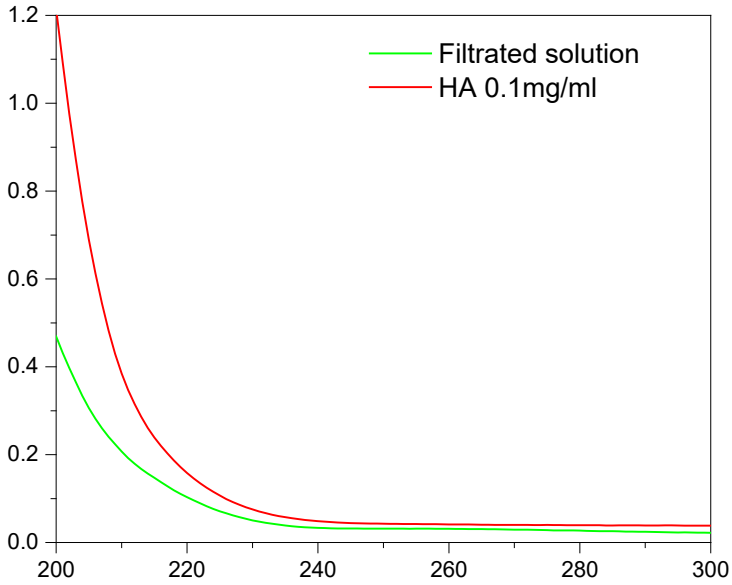

Figure S1: Absorbance of filtering solution of HACNT membrane (green), comparing with 0.1mg/mL HA solution (red).

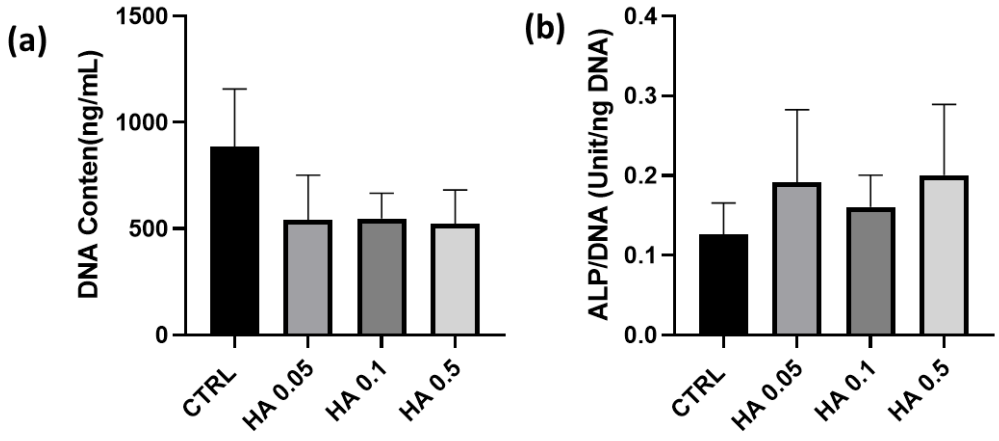

Figure S2: (a) DNA content and (b) ALP activity of mBMCs culture in culture medium with 0.05, 0.1. 0.5 mg/mL hyaluronic acid solution after 7 days (n=5).

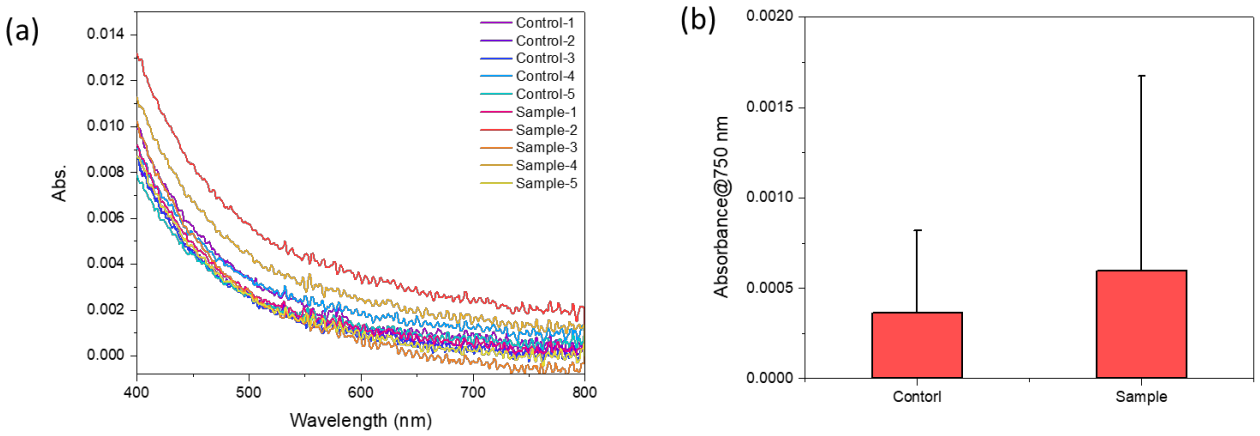

Figure S3: Absorbance of PBS solution with HACNT membrane immersed after 8 weeks at room temperature and pressure (n=5). (a) Baseline corrected graph of values at 800 nm. (b) Graph comparing the baseline corrected 800 nm value to the 750 nm value.

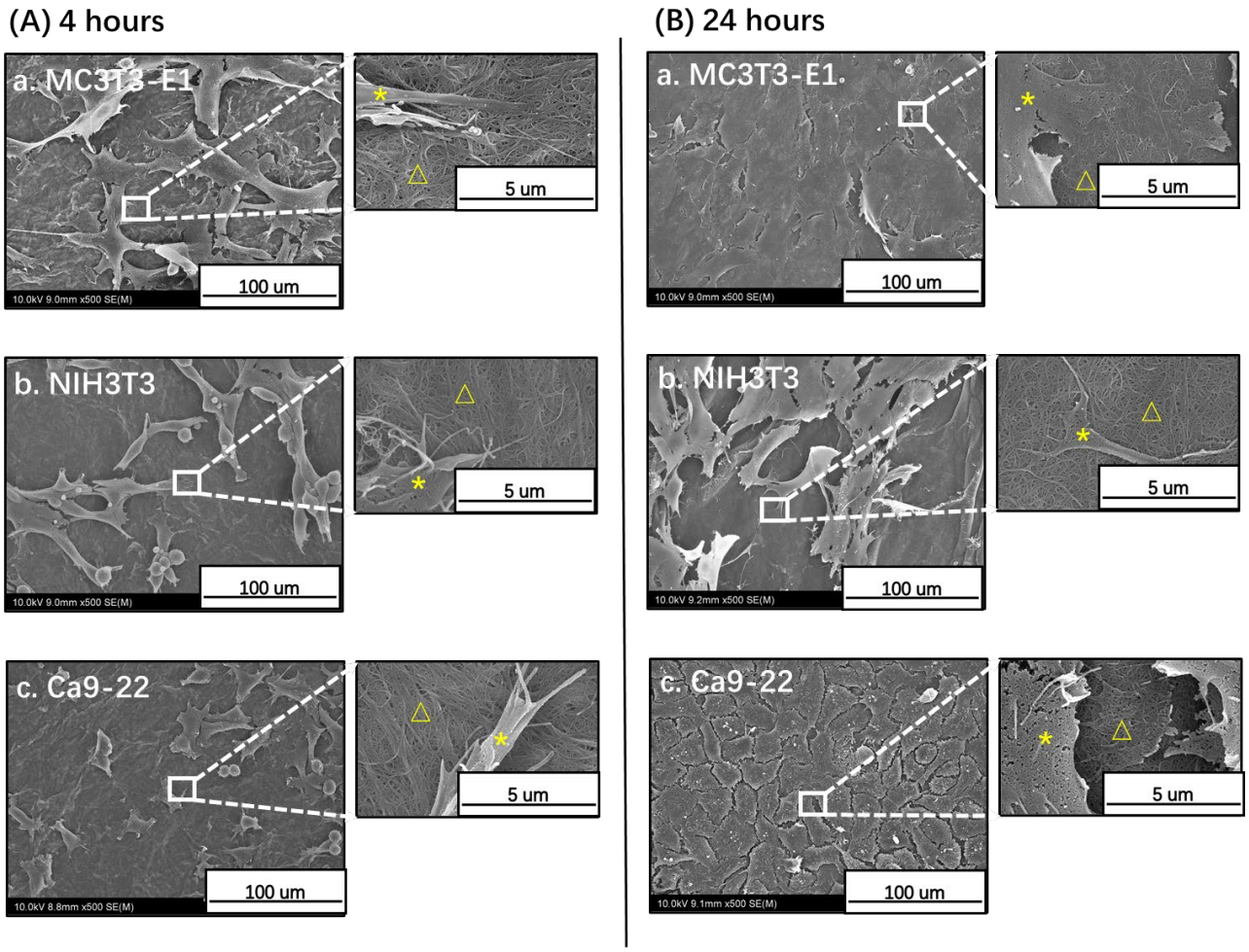

Figure S4. SEM observations of MC3T3-E1, NIH3T3 and Ca9-22 cells cultured on HACNT membrane after 4 and 24 hours. Asterisk: cell. Triangle: HACNT membrane.

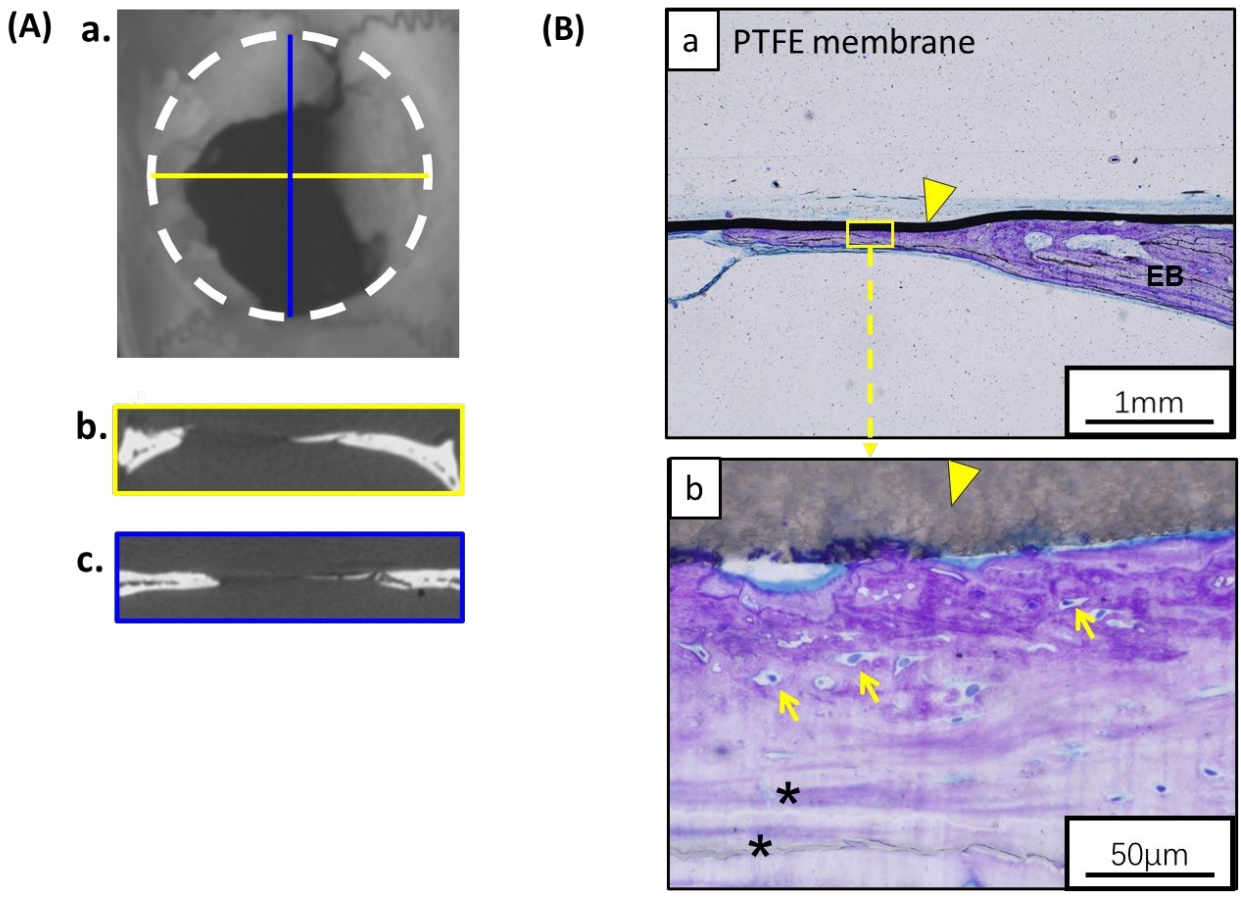

Figure S5. (A) Micro-CT images of representative rat's calvarial bone samples with PTFE membrane implantation after 8 weeks. (a): horizontal plane. (b): coronal plane. (c): sagittal plane . (B) Representative histological sections of rat PTFE implantation after 8 weeks. (a) Thin bone tissue was formed from existing bone (EB) under PTFE membrane (yellow arrowhead). (b) Some part of new bone with osteocytes (yellow arrow) were attached to PTFE membrane (yellow arrowhead) directly. Lamellar structure (asterisk) was observed lower part of newly formed bone.